Chemical Physics Letters 884 (2026) 142600

Contents lists available at ScienceDirect

Chemical Physics Letters

journal homepage: www.elsevier.com/locate/cplett

Densification processes of crystalline purine: Negative linear compressibility and pressure-induced phase transition

Hiroki Kobayashi *, Kazuki Komatsu, Hiroyuki Kagi

Geochemical Research Center, Graduate School of Science, The University of Tokyo, 7-3-1, Hongo, Bunkyo-ku, Tokyo 113-0033, Japan

ARTICLE INFO

Keywords:
Negative linear compressibility
High pressure
Phase transition
X-ray diffraction
Hydrogen bonds

ABSTRACT

We investigated the densification mechanisms of crystalline purine at room temperature using powder and single-crystal x-ray diffraction under quasi-hydrostatic pressure. The ambient orthorhombic phase exhibits negative linear compressibility until it transforms at 0.7–1.1 GPa into a newly reported high-pressure polymorph. This phase transition can be explained by flipping and translation of hydrogen-bonded molecular arrays. Judging from interatomic distances, intermolecular N–H…N hydrogen bonds in the high-pressure phase are weakened but doubled, leading to an efficient densification.

Molecular crystals have been studied from various aspects, from fundamental physics and chemistry to applications as pharmaceuticals, gas- and energy-storage materials, electronic and optical devices, and so on. In particular, hydrogen-bonded systems often show intriguing properties because the flexibility of hydrogen bonds allows various structural and dynamic features that appear, for example, as polymorphism. Purine ($C_5H_4N_4$) is an important building block of DNA and also an interesting research subject in chemical physics. In its crystal structure, nearly flat purine molecules form intermolecular N-H…N hydrogen bonds, which lead to structural anisotropy. Variable temperature terahertz spectroscopy has shown strong anharmonicity in the vibrational potentials of purine [1,2]. This is related to its highly anisotropic thermal expansion arising from the planar molecular structure [3] and therefore, interesting anisotropic pressure responses are also expected since hydrogen bonds are flexible and readily modulated by pressure but covalent bonds are kept rigid. Understanding the densification processes of purine under high pressure would provide fundamental physicochemical insights into pressure responses of hydrogen-bonded molecular crystals.

The crystal structure of the ambient phase of purine was reported by Watson, Sweet, and Marsh in 1965, illustrated in Fig. 1 (CCDC deposition numbers: 1239746 and 1239747) [4,5]. Our starting material was confirmed to have the same structure as reported in the literature based on both single-crystal and powder x-ray diffraction. The structure is orthorhombic and has the $Pna2_1$ space group symmetry, but in this article, we changed the setting to the non-standard $P2_1nb$ [setting No. 3 for $Pna2_1$], aiming at a straightforward comparison between the ambient and a high-pressure phase newly identified by us. The structure consists of hydrogen-bonded molecular arrays, for which two arrays are alternately arranged in different orientations. As apparently seen when viewed along the *b*-axis (Fig. 1(c)), each molecule has a neighbouring molecule in the other type of array along the *b*-axis direction. The hydrogen-bonded pair of molecules is not parallel to each other but slightly inclined (Fig. 1(d)).

We investigated the pressure-induced structural changes of crystalline purine using x-ray diffraction. Fig. 2(a) shows powder diffraction patterns along hydrostatic compression in Daphne 7575 pressure-transmitting medium [6] at room temperature, collected using synchrotron x-rays and a diamond anvil cell. Two-dimensional x-ray diffraction patterns were fairly but not perfectly smooth for Rietveld analyses, and no pronounced preferred orientation effects were confirmed. The ambient orthorhombic phase was observed up to ~1 GPa, followed by a pressure-induced phase transition into an unknown high-pressure phase. As described in detail later, this phase transition is observed above 0.7 GPa but is sluggish, making the ambient phase observable even above 1 GPa in powder diffraction experiments completed within a few hours. The ambient phase exhibited negative linear compressibility (NLC) along the *c*-axis as seen in the high-*d* shifts of the 002 reflection with increasing pressure (Fig. 2(b) and 2(c)). Fig. 2(d) summarises the axial compressibility and the fitted curves using an empirical formula of $x(p) = x_0 + \lambda(p - p_c)^{\nu}$ [7–10]. It is noted here that the *c*-axis shows negative thermal expansion (NTE) according to single-crystal diffraction studies at ambient pressure by Ruggiero et al. [3] from single-crystal x-ray diffraction at 1 atm. This is consistent with the fact that NLC materials frequently exhibit NTE or highly anisotropic thermal expansion. These NLC and NTE behaviour can be described by a rotation of

* Corresponding author.
E-mail address: hiroki@eqchem.s.u-tokyo.ac.jp (H. Kobayashi).

https://doi.org/10.1016/j.cplett.2025.142600
Received 18 November 2025; Received in revised form 1 December 2025; Accepted 10 December 2025
Available online 11 December 2025

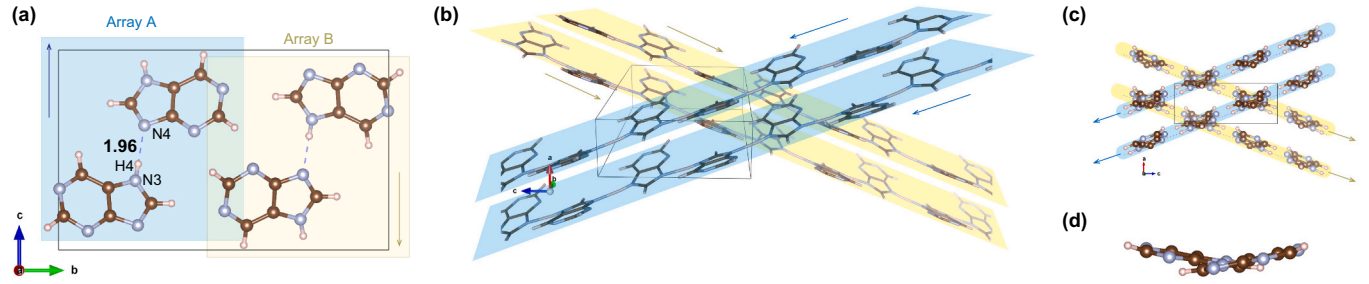

Fig. 1. Packing structure of the purine ambient phase (Space group: $P2_1nb$ [No. 33, setting No. 3]). (a) The unit-cell structure viewed along the *a*-axis, highlighting the N3-H4…N4 intermolecular hydrogen bonds. The structure can be described by two stacked hydrogen-bonded molecular arrays (Arrays A & B) shown by blue and yellow rectangles. The direction of each array is defined as shown by arrows according to the hydrogen-bond donor-to-acceptor vector. (b–c) Relation between two molecular arrays. (d) Intra-array structure viewed along the intermolecular hydrogen-bond direction. The hydrogen-bonded molecules are not perfectly parallel. (For interpretation of the references to colour in this figure legend, the reader is referred to the web version of this article.)

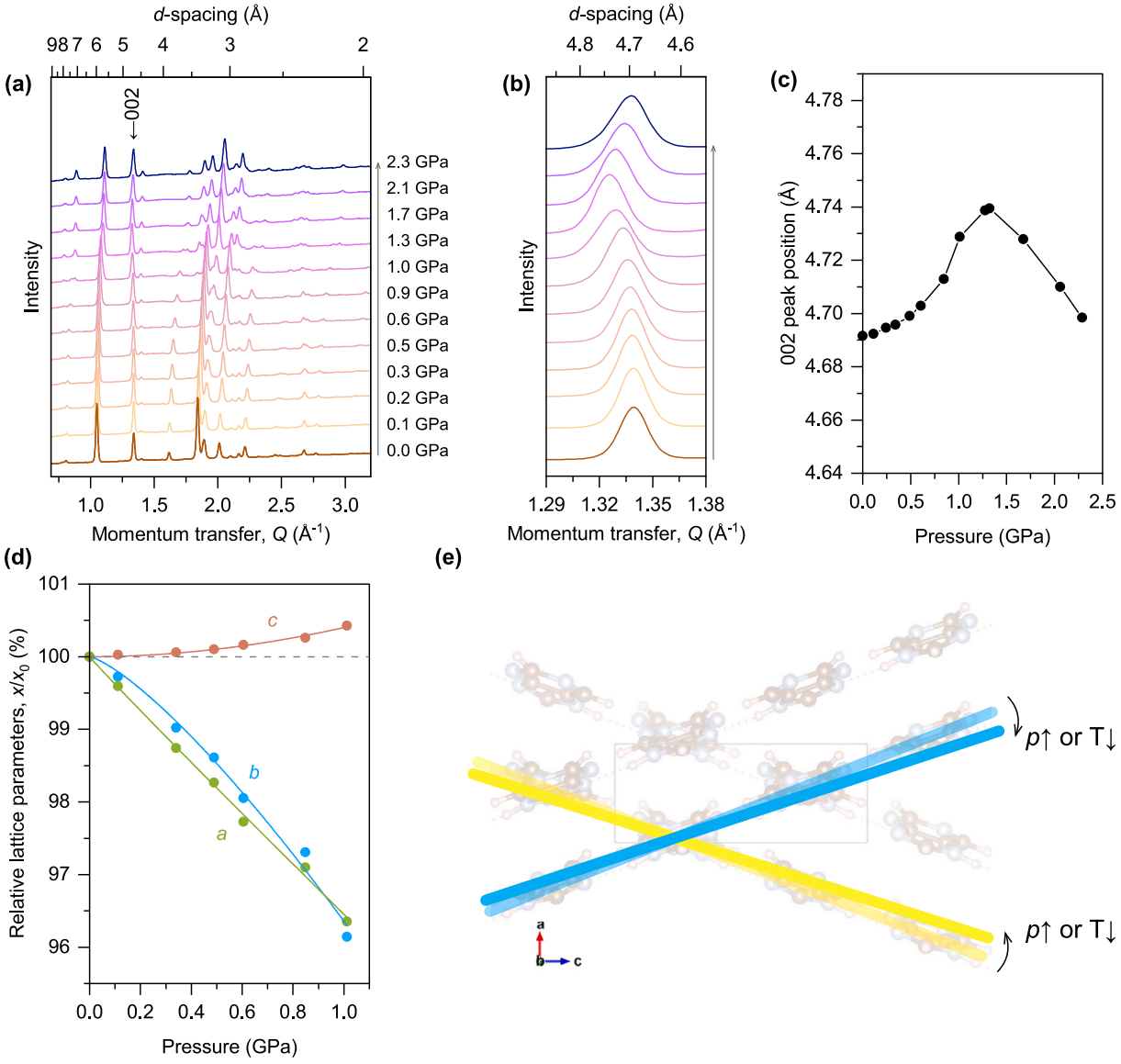

Fig. 2. Powder x-ray diffraction at high pressures. (a) Diffraction profiles with increasing pressure. (b) Enlarged 002 reflection. (c) *d*-values of the 002 reflection as a function of pressure calculated by single-peak fitting using pseudo-Voigt functions. (d) Lattice parameters relative to the values at 1 atm as functions of pressure. Curves represent the fitting results using an empirical formulation of $x(p) = x_0 + \lambda(p - p_c)^{\nu}$. Since p_c was found to be extremely close to zero, we fixed it to exact zero. x_0 was also fixed to the value obtained at 1 atm. Fitted values: (*a*-axis) $\lambda = -0.132$ (4), $\nu = 1.06(8)$; (*b*-axis) $\lambda = -0.566$ (19), $\nu = 1.35(9)$; (*c*-axis) $\lambda = 0.038(2)$, $\nu = 1.98(21)$. (e) Schematic illustration of the densification mechanism in the ambient phase upon compression and cooling.

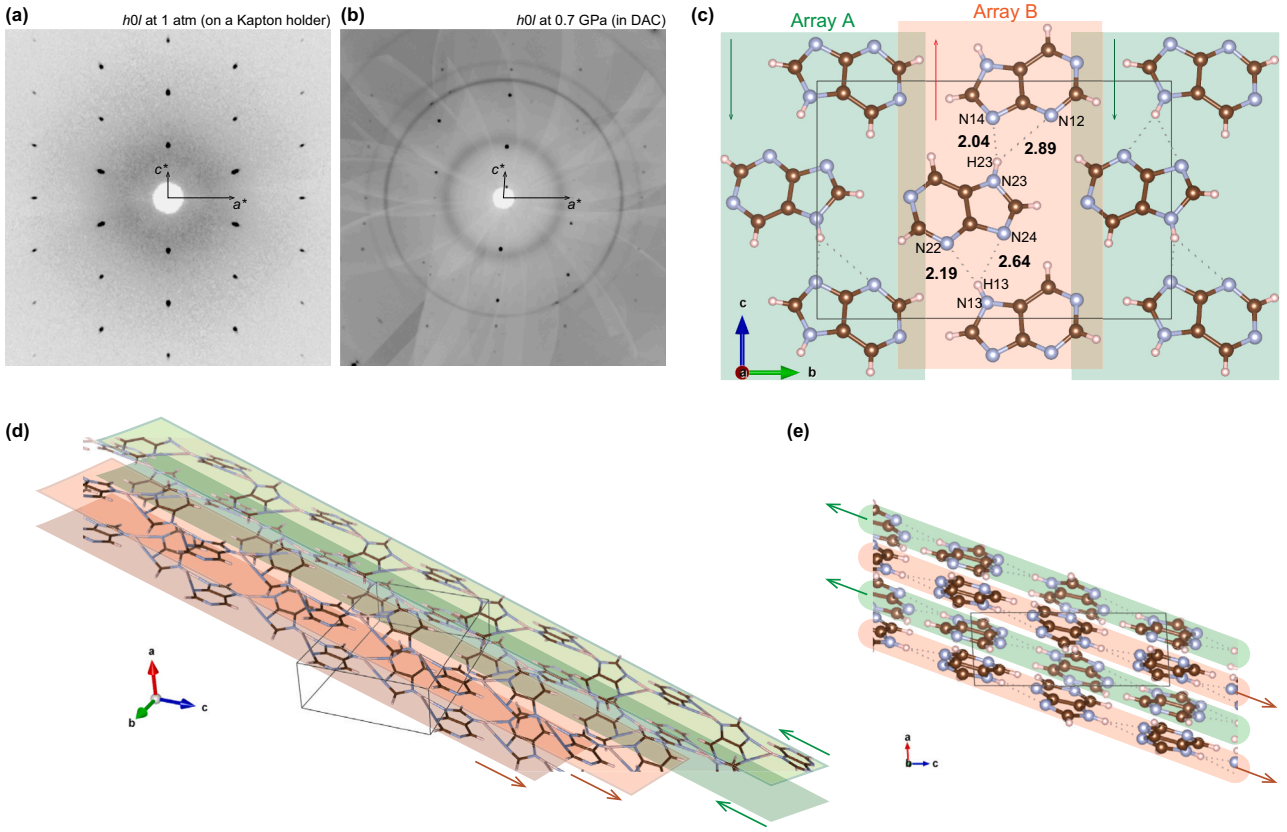

Fig. 3. Structure of the high-pressure phase. (a-b) Reconstructed reciprocal *h0l* plane of the ambient (a) and high-pressure (b) phases. (c) Structure of the high-pressure phase viewed along the *a*-axis. (d-e) Arrangement of the molecular arrays in the high-pressure phase.

the molecular arrays, as schematically illustrated in Fig. 2(e).

These axial compressibilities of the ambient phase are consistent, at least qualitatively, with a DFT-D3(BJ) prediction of the compressibility of purine reported by Fedorov and Korabelnikov [11]. Especially, the pressure responses of the NLC axis (*c*-axis in our setting, *b*-axis in the setting in Ref. [11]) are in quantitative agreement between experiments and calculations. However, their calculations underestimated the compressibility of the *b*-axis (the *a*-axis in Ref. [11]) and overestimated that of the *a*-axis (the *c*-axis in Ref. [11]). In experiments, $a/a_{0\ \mathrm{GPa}}$ and $b/b_{0\ \mathrm{GPa}}$ showed similar decreasing trends with pressure, reaching ~96.5% at 1 GPa. In DFT calculations by Fedorov and Korabelnikov [11], on the other hand, $a/a_{0\ \mathrm{GPa}}$ and $b/b_{0\ \mathrm{GPa}}$ ($c/c_{0\ \mathrm{GPa}}$ and $a/a_{0\ \mathrm{GPa}}$ in Ref. [11]) showed anisotropic compaction, reaching ~95% and ~ 98% at 1 GPa, respectively. Our experimental data can be used as a benchmark for DFT computation for purine. A higher-level dispersion correction, such as DFT-D4 [12] and the many-body dispersion (MBD) [13] method, might improve the calculations since weak interactions are important in this system.

On further compression, purine underwent a pressure-induced phase transition at $p > 0.7$ GPa, although the ambient phase was observable up to ~1.1 GPa along the compression pathway. We found that the minimum pressure required for the appearance of the high-pressure phase was 0.7 GPa, but the transition was very slow. Therefore, the ambient phase remained even above 0.7 GPa in the presented powder diffraction data, where the experiment was completed within a few hours. For single-crystal diffraction measurements above 0.7 GPa, we spent at least 12 h before starting measurements to avoid changes in the crystal structure during diffraction measurements. On decompression, the high-pressure phase underwent a transition back to the ambient phase around 0.2 GPa, but was not recoverable to ambient pressure. Based on these observations, we suggest that the crossover of the thermodynamic stability of the ambient and high-pressure phases occurs between 0.2 and 0.7 GPa (the onset pressures of decompression- and compression-induced phase transitions). The exact value may be estimated by theoretically calculating the enthalpies of these phases as functions of pressure. In the "overcompressed" pressure region of 0.7–1.1 GPa, the ambient phase showed abrupt changes in its pressure responses, likely due to its metastability. For example, the pressure-induced shift of the 002 reflection (Fig. 2(c)) got more marked above 0.7 GPa.

The structure of the newly discovered high-pressure polymorph was solved by single-crystal x-ray diffraction using a diamond anvil cell (DAC) equipped with Boehler-Almax design anvils and a custom-made seat that provides a maximum opening angle of $2\theta = 65°$ [14,15]. The pressure-induced phase transition was observed in a single-crystal-to-single-crystal manner (twinning was observed in some runs). The high-pressure phase was identified to have a similar unit cell to the ambient phase but with a reduced monoclinic lattice symmetry. Single-crystal x-ray diffraction patterns (Fig. 3(a)(b)) provide evidence for the monoclinic distortion with $\beta \sim 93°$. In diffraction patterns, the series of 0 *k*0 reflections was inaccessible due to the geometry of the diamond anvil cell, making it difficult to judge the presence or absence of the systematic extinction originating from 2_1 screw axes. We tried measurements with several different samples, but the 0*k*0 series was inaccessible in all trials; we tried to measure a crystal in a completely different orientation, but purine crystals are needle-shaped, making it difficult to arrange such crystals so that their elongated direction aligned with the pressurisation axis of the DAC. Aiming at the structural analysis with limited coverage of the reciprocal space, we prepared reflection tables without considering any reflection conditions arising from point group symmetry. Therefore, symmetry-free phasing was followed by symmetry search in the obtained electron density using the *SHELXT* suite [16], and we obtained a plausible structural model having the $P2_1$ space group. $P2_1$ (*i.e.* $P12_11$) is not a subgroup of the original space group of the ambient phase, $P2_1nb$, although the unit cell dimensions are similar between the ambient and high-pressure phases. As this indicates,

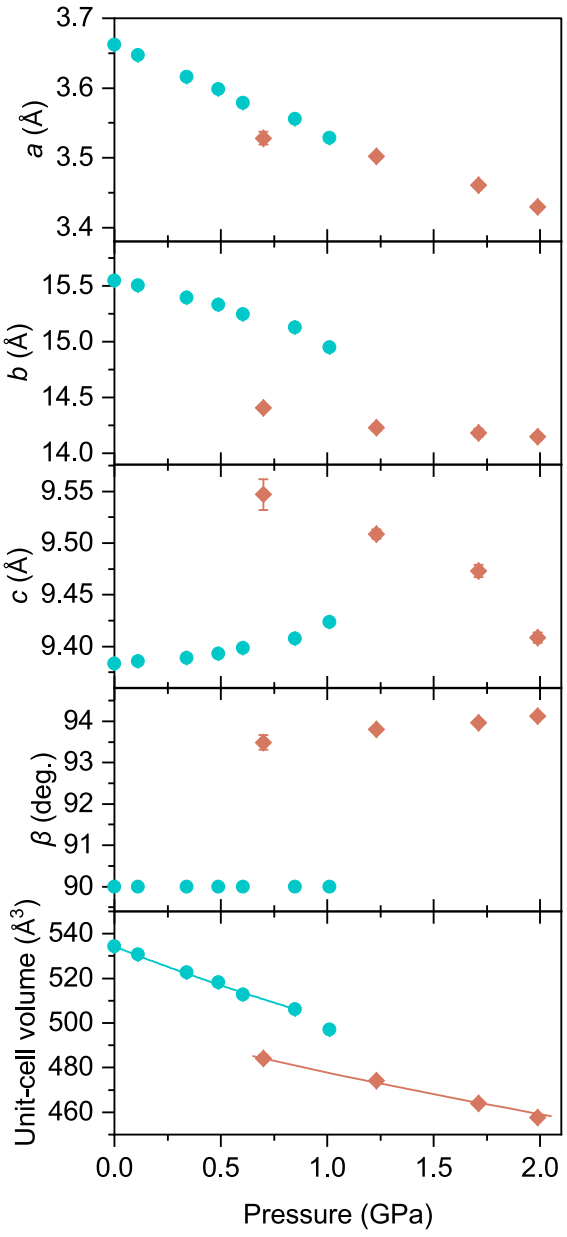

Fig. 4. Lattice parameters of the ambient phase (blue circles, from powder diffraction) and the high-pressure phase (red diamonds, from single-crystal diffraction. Solid curves for the unit-cell volume represent second-order Birch-Murnaghan equation-of-state (EoS) fits. Ambient phase: V_0 = 534.244 (22) Å^3 (determined from diffraction data at 1 atm by Le Bail fitting and fixed in the EoS fitting), K_0 = 14.2(3) GPa, K_0' = 4. High-pressure phase: V_0 = 500.7 (14) Å^3, K_0 = 19.5(9), K_0' = 4. (For interpretation of the references to colour in this figure legend, the reader is referred to the web version of this article.)

the structure of the high-pressure polymorph is indeed not explained by simple loss of symmetry operations but rather involves drastic changes in the packing structure. It is interesting that a single-crystal-to-single-crystal transition was possible, for which the clear reason is yet unknown. The refined structure is illustrated in Fig. 3. In the ambient phase, two molecular arrays (Arrays A & B) form a crossing structure when viewed along the *b*-axis (Fig. 1(b)), whilst in the high-pressure phase, each array is nearly parallel to the other (Fig. 3(d)(e)). Arrays A and B were oriented upwards and downwards relative to the *a*-axis direction in the ambient phase, but in the high-pressure phase, both are aligned downwards (or upwards).

This phase transition involves approximately 5% reduction of the unit-cell volume associated with anisotropic changes in axis dimensions, where the NLC axis (the *c*-axis) showed a notable expansion, and the *b*-axis is significantly shortened (Fig. 4). No axes showed negative compressibility in the high-pressure phase, but a 'rotating array' densification mechanism, similar to the ambient phase, was present as evidenced by a slight increase in the β angle with increasing pressure.

Judging from interatomic distances, the high-pressure phase is highly likely to be stabilised by additional N-H…N hydrogen-bond interactions. In Fig. 3(c), four crystallographically inequivalent N-H…N lengths are shown. In the ambient phase, only N13-H13…N24 and N23-H23…N14 form hydrogen bonds, whilst in the high-pressure phase, two additional nitrogen atoms, namely N22 and N12, become close enough to form a hydrogen bond (d(N—N) < 3.5 Å / d(H…N) < 2.5 Å, *e.g.*, [17–19]). Given the uncertainties in the interatomic distances as well as the nature of very weak hydrogen bonds, further evidence from spectroscopic experiments and theoretical calculations is highly desired, although our Raman spectroscopic attempts were unsuccessful due to the strong fluorescence of purine. On the other hand, each N-H…N hydrogen bond in the high-pressure phase is longer than that in the ambient phase (d(H…N) = 1.96 Å), indicating that it is not as strong as in the ambient pressure. In the high-pressure phase, two adjacent arrays (Array A and B) are stacked alternately along the *a*-axis. This can be interpreted as having the effect of reducing repulsion between molecules adjacent along the *b*-axis. Consequently, the distance between hydrogen-bonding molecules along the *b*-axis (the "width" of the arrays along the *b*-axis) decreases, enabling two nitrogen atoms to contribute to hydrogen bonding. While this weakens each hydrogen bond, the simultaneous reduction in spatial repulsion between molecules allows for the efficient formation of a denser structure, facilitating the pressure-induced phase transition.

Summarising these crystallographic considerations, the pressure-induced phase transition in purine can be explained by three mechanisms: (i) Array B aligns in the same direction as Array A relative to the

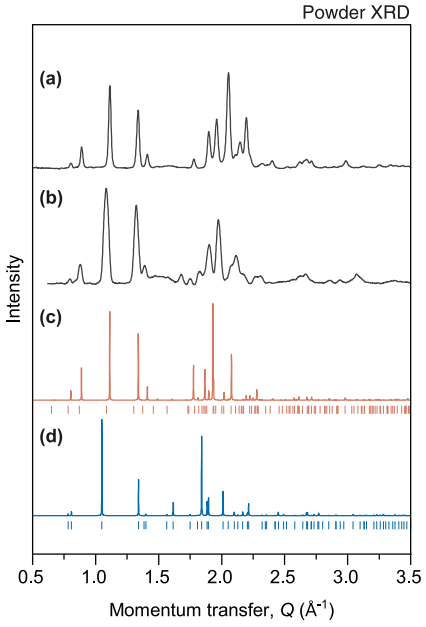

Fig. 5. Comparing powder diffraction profiles of the high-pressure phase. The background was subtracted manually for experimental data, and all patterns were normalised. (a) Experimental powder x-ray diffraction profile of a purine sample compressed to 2.73 GPa within 3 h and then decompressed to 0.7 GPa, collected using synchrotron x-rays at BL-18C. (b) Experimental powder x-ray diffraction profile of a purine sample compressed quickly within 1 min to 0.7 GPa and then left there for 2 days, collected using laboratory-source Mo $K\alpha$ radiation. (c) Simulated powder x-ray diffraction profile of the high-pressure phase based on our structure model by single-crystal diffraction. (d) Simulated powder x-ray diffraction profile of the ambient phase for reference.

a-axis direction, (ii) Array B undergoes a 1/2 parallel shift along the *a*-axis direction, thereby reducing inter-array repulsion, and (iii) molecules within the arrays shift (nearly) parallel to the *b*-axis direction, forming elongated but doubled intermolecular hydrogen bonds. Crystallographically, the 2_1 axis parallel to the *a*-axis disappears, and new 2_1 axis parallel to the *b*-axis appears. In-array molecules become symmetry inequivalent in the high-pressure polymorph, doubling the crystallographic sites required to describe the packing structure.

The potential formation of weakened but doubled hydrogen bonds is a distinctive pressure response in purine crystals arising from its molecular structure. Watson, Sweet, and Marsh (1965) reported that the packing structure of the ambient phase of purine was similar to that of pyrimidine ($C_4N_2H_4$, reported by Wheatley in 1960), sharing the same space group and nearly identical *a* and *c* dimensions [4,20]. However, pyrimidine is apparently not capable of forming an additional hydrogen bond as purine does at high pressures, which raises the possibility that these two compounds differ significantly in terms of the densification processes upon compression. Comprehensive high-pressure experiments on pyrimidine-group crystals in the future may reveal the generalised relationship between molecular structure and the mechanism of densification.

Lastly, we note that the pressure-induced phase transition in crystalline purine involves complicated kinetic pathways, and the structural model obtained by single-crystal diffraction may not perfectly describe the structural changes occurring in compressed polycrystalline (powder) samples. Fig. 5 summarises the experimental powder x-ray diffraction profiles and simulated patterns using the structure models by single-crystal diffraction (simulated by VESTA [21]). Some peaks are absent or weak in the simulated pattern but relatively intense in experimental ones, along with some peak intensities that are unmatched. We have not succeeded in indexing this powder pattern. Rietveld analysis using the structure model from single-crystal diffraction was unsuccessful, for which a representative fitting attempt is shown in the Supplementary Information (Fig. S1). Furthermore, there are also differences between experimental profiles (Fig. 5(a)(b)). Fig. 5(a) shows the powder x-ray diffraction profile of a purine sample compressed to 2.73 GPa within 3 h and then decompressed to 0.7 GPa, whilst Fig. 5(b) is the powder x-ray diffraction profile of a purine sample compressed quickly within 1 min from 0 to 0.7 GPa and then kept at this pressure for 2 days (intensities are normalised using the highest peak). These two patterns are clearly different in terms of peak intensities, and they are not likely simple mixtures of the ambient and high-pressure phases, as an "addition" of the ambient-phase profile did not resolve this discrepancy. Although such powder/single-crystal mismatch is a frequent observation in crystallography, our observations imply the presence of intermediate structure(s) in the kinetically complex structural transformation pathways from the ambient to high-pressure polymorphs. These intermediate structures would be an interesting subject for future studies.

In summary, we investigated pressure-induced structural responses of crystalline purine at room temperature. The ambient orthorhombic phase exhibited NLC, followed by a phase transition into a newly reported high-pressure monoclinic polymorph at pressures between 0.7 and 1.1 GPa. The N–H…N hydrogen bonds are elongated but likely to be doubled in the high-pressure phase, contributing to the efficient achievement of a dense packing structure. Powder diffractograms indicate that this pressure-induced phase transition is sluggish, involving several intermediate structures that were not captured in single-crystal diffraction. We anticipate that a better understanding of the densification mechanism of other related compounds would lead to generalised knowledge about the relationship between the molecular and packing structures as a function of pressure.

CRediT authorship contribution statement

Hiroki Kobayashi: Writing – original draft, Visualization, Project administration, Investigation, Formal analysis, Data curation, Conceptualization. **Kazuki Komatsu:** Writing – review & editing, Supervision, Investigation, Formal analysis. **Hiroyuki Kagi:** Writing – review & editing, Supervision, Investigation.

Declaration of competing interest

The authors declare that they have no known competing financial interests or personal relationships that could have appeared to influence the work reported in this paper.

Acknowledgements

We express our deep appreciation to Akio Yasuda (The University of Tokyo) for contributing to preliminary measurements, which triggered this project. Synchrotron x-ray diffraction experiments were carried out at BL-18C in the Photon Factory of High-Energy Accelerator Research Organization (KEK) (Proposal No.: 2023G145). We thank Yuki Shibazaki and Kazuki Watanabe (KEK) for their help in experiments at BL-18C. H. Kobayashi is a recipient of financial support from the MERIT-WINGS programme (The University of Tokyo), the Ludo Frevel Crystallography Scholarship Award 2025 (International Centre for Diffraction Data), and the Overseas Challenge Program for Young Researchers (JSPS: Japan Society for the Promotion of Science). This work was supported by JSPS Grants-in-Aid for Scientific Research '*KAKENHI*' (Grant No.: 23H00140 and 21K18643). Structure visuals were generated using the VESTA software [21].

Appendix A. Supplementary data

Supplementary data to this article can be found online at https://doi.org/10.1016/j.cplett.2025.142600.

Data availability

Data will be made available on request.

References

[1] Y.C. Shen, P.C. Upadhya, E.H. Linfield, A.G. Davies, Temperature-dependent low-frequency vibrational spectra of purine and adenine, Appl. Phys. Lett. 82 (2003) 2350–2352, https://doi.org/10.1063/1.1565680.
[2] M.T. Ruggiero, J.A. Zeitler, Resolving the origins of crystalline anharmonicity using terahertz time-domain spectroscopy and ab initio simulations, J. Phys. Chem. B 120 (2016) 11733–11739, https://doi.org/10.1021/acs.jpcb.6b10248.
[3] M.T. Ruggiero, J.A. Zeitler, A. Erba, Intermolecular anharmonicity in molecular crystals: interplay between experimental low-frequency dynamics and quantum quasi-harmonic simulations of solid purine, Chem. Commun. 53 (2017) 3781–3784, https://doi.org/10.1039/C7CC00509A.
[4] D.G. Watson, R.M. Sweet, R.E. Marsh, The crystal and molecular structure of purine, Acta Crystallogr. 19 (1965) 573–580, https://doi.org/10.1107/S0365110X65003900.
[5] B. Pullman, H. Berthod, J. Caillet, On the crystal structure of purine, Theor. Chim. Acta 10 (1968) 43–46, https://doi.org/10.1007/BF00529042.
[6] D. Staško, J. Prchal, M. Klicpera, S. Aoki, K. Murata, Pressure media for high pressure experiments, Daphne oil 7000 series, High Pressure Res. 40 (2020) 525–536, https://doi.org/10.1080/08957959.2020.1825706.
[7] A.L. Goodwin, D.A. Keen, M.G. Tucker, Large negative linear compressibility of $Ag_3[Co(CN)_6]$, Proc. Natl. Acad. Sci. USA 105 (2008) 18708–18713, https://doi.org/10.1073/pnas.0804789105.
[8] M.J. Cliffe, A.L. Goodwin, PASCal: a principal axis strain calculator for thermal expansion and compressibility determination, J. Appl. Crystallogr. 45 (2012) 1321–1329, https://doi.org/10.1107/S0021889812043026.
[9] A.B. Cairns, A.L. Thompson, M.G. Tucker, J. Haines, A.L. Goodwin, Rational design of materials with extreme negative compressibility: selective soft-mode frustration in $KMn[Ag(CN)_2]_3$, J. Am. Chem. Soc. 134 (2012) 4454–4456, https://doi.org/10.1021/ja204908m.
[10] A.B. Cairns, A.L. Goodwin, Negative linear compressibility, Phys. Chem. Chem. Phys. 17 (2015) 20449–20465, https://doi.org/10.1039/c5cp00442j.
[11] I.A. Fedorov, D.V. Korabelnikov, Ab initio study of the compressibility and electronic properties of crystalline purine, J. Struct. Chem. 63 (2022) 1670–1677, https://doi.org/10.1134/S0022476622100134.
[12] E. Caldeweyher, J.M. Mewes, S. Ehlert, S. Grimme, Extension and evaluation of the D4 London-dispersion model for periodic systems, Phys. Chem. Chem. Phys. 22 (2020) 8499–8512, https://doi.org/10.1039/d0cp00502a.
[13] A. Tkatchenko, R.A. Distasio, R. Car, M. Scheffler, Accurate and efficient method for many-body van der Waals interactions, Phys. Rev. Lett. 108 (2012), https://doi.org/10.1103/PhysRevLett.108.236402.
[14] K. Komatsu, H. Kagi, T. Yasuzuka, T. Koizumi, R. Iizuka, K. Sugiyama, Y. Yokoyama, A design of backing seat and gasket assembly in diamond anvil cell

for accurate single crystal x-ray diffraction to 5 GPa, Rev. Sci. Instrum. 82 (2011) 105107, https://doi.org/10.1063/1.3646460.
[15] K. Yamashita, K. Komatsu, H. Kagi, Crystal structure of potassium chloride monohydrate: water intercalation into the B1 structure of KCl under high pressure, Acta Crystallogr C, Struct. Chem. 78 (2022) 749–754, https://doi.org/10.1107/S2053229622011135.
[16] G.M. Sheldrick, SHELXT – integrated space-group and crystal-structure determination, Acta Crystallogr A Found Adv 71 (2015) 3–8, https://doi.org/10.1107/S2053273314026370.
[17] R.N.V. Krishna Deepak, R. Sankararamakrishnan, Unconventional N-H...N hydrogen bonds involving proline backbone nitrogen in protein structures, Biophys. J. 110 (2016) 1967–1979, https://doi.org/10.1016/j.bpj.2016.03.034.
[18] E.N. Baker, R.E. Hubbard, Hydrogen bonding in globular proteins, Prog. Biophys. Mol. Biol. 44 (1984) 97–179, https://doi.org/10.1016/0079-6107(84)90007-5.
[19] E.Yu. Tupikina, M. Sigalov, I.G. Shenderovich, V.V. Mulloyarova, G.S. Denisov, P. M. Tolstoy, Correlations of NHN hydrogen bond energy with geometry and 1H NMR chemical shift difference of NH protons for aniline complexes, J. Chem. Phys. 150 (2019) 114305, https://doi.org/10.1063/1.5090180.
[20] P.J. Wheatley, The crystal and molecular structure of pyrimidine, Acta Crystallogr. 13 (1960) 80–85, https://doi.org/10.1107/S0365110X60000200.
[21] K. Momma, F. Izumi, VESTA 3 for three-dimensional visualization of crystal, volumetric and morphology data, J. Appl. Crystallogr. 44 (2011) 1272–1276, https://doi.org/10.1107/S0021889811038970.